X-ray photoelectron spectroscopy analysis of GaN/(0001)AlN and AlN/(0001)GaN growth mechanisms

Cite as: Journal of Applied Physics **86**, 5584 (1999); https://doi.org/10.1063/1.371564
Submitted: 01 March 1999 • Accepted: 06 August 1999 • Published Online: 01 November 1999

S. W. King, E. P. Carlson, R. J. Therrien, et al.

X-ray photoelectron spectroscopy analysis of GaN/(0001)AlN and AlN/(0001)GaN growth mechanisms

S. W. King, E. P. Carlson, and R. J. Therrien
Department of Materials Science and Engineering, Campus Box 7907, North Carolina State University, Raleigh, North Carolina 27695

J. A. Christman and R. J. Nemanich
Department of Physics, Campus Box 8202, North Carolina State University, Raleigh, North Carolina 27695

R. F. Davis[a)]
Department of Materials Science and Engineering, Campus Box 7907, North Carolina State University, Raleigh, North Carolina 27695

(Received 1 March 1999; accepted for publication 6 August 1999)

The mechanisms of growth of GaN on AlN and AlN on GaN via gas source-molecular beam epitaxy with NH_3 as the nitrogen source have been investigated using x-ray photoelectron spectroscopy, low energy electron diffraction, and Auger electron spectroscopy. The growth of GaN on AlN at low temperatures (650–750 °C) occurs via a Stranski–Krastanov 2D→3D type mechanism with the transition to 3D growth occurring at ≈10–15 Å. The mechanism changes to Frank van der Merwe (FM)/layer-by-layer growth above 800 °C. The growth of AlN on GaN occurred via a FM layer-by-layer mechanism within the 750–900 °C temperature range investigated. We propose a model based on the interaction of ammonia and atomic hydrogen with the GaN/AlN surfaces which indicates that the surface kinetics of hydrogen desorption and ammonia decomposition are the factors that determine the GaN growth mechanism. © *1999 American Institute of Physics.* [S0021-8979(99)08521-7]

I. INTRODUCTION

Gallium nitride (GaN) and aluminum nitride (AlN) are completely miscible semiconductors with band gaps of 3.45 and 6.2 eV, respectively. Several commercial applications for these materials including UV-visible/optoelectronic and high-power, high-frequency, and high-temperature microelectronic devices have been realized.[1–7] To date, the two most popular techniques for growth of these materials have been organometallic vapor phase epitaxy (OMVPE) and plasma-assisted electron cyclotron resonance or radio-frequency induced gas source molecular beam epitaxy (PAGSMBE). The success and improved understanding of the OMVPE and PAGSMBE techniques have been greatly aided by several studies of the growth mechanisms of GaN and AlN on various substrates by these techniques.[8–17] An alternative to OMVPE and PAGSMBE growth of GaN is reactive molecular beam epitaxy which essentially replaces the electron cyclotron resonance (ECR) or rf N_2 source with NH_3 in the MBE system (i.e., NH_3–GSMBE). This last technique is currently gaining increased employment due to its inherent simplicity relative to PAGSMBE, the markedly increased purity of commercially available NH_3, and the improved electrical and optical properties of GaN films grown by this technique.[18–24]

Yoshida *et al.*[25–29] were the first to report the growth of films of AlN, GaN, and $Al_xGa_{1-x}N$ alloys by NH_3–GSMBE. Highly resistive and single crystalline [as determined by reflection high-energy electron diffraction (RHEED)] AlN films were achieved on (0001) and $(11\bar{2}0)$ Al_2O_3 substrates at 1000 and 1100 °C, respectively.[25,26] By contrast, the GaN films were grown at 700 °C on (0001) Al_2O_3 and were highly conductive with carrier concentrations of 10^{19}–$10^{20}/cm^3$ and mobilities of 30 $cm^2/V\,s$.[27] The growth of an AlN buffer layer between the GaN and the Al_2O_3 did not change the electrical properties of their films. However, these investigators did make the key observation[28,29] that the band edge cathodoluminescence (CL) intensities from the latter GaN films were 25 times greater than those from films grown directly on Al_2O_3.

Subsequent research has resulted in a steady improvement in the desired structural, chemical, and electrical properties of the GaN films grown by NH_3–MBE. Films grown directly on (0001) Al_2O_3 by Powell, Lee, and Greene[30] at 760–780 °C exhibited carrier concentrations of $1-4\times10^{18}/cm^3$ and mobilities of 100–110 $cm^2/V\,s$. A further reduction in carrier concentration to $2\times10^{17}/cm^3$ has been demonstrated by Yang, Li, and Wang[18,19] and Kamp *et al.*[21] by the use of an AlN buffer layer on (0001) Al_2O_3. Through optimization of the NH_3 flux, Kim *et al.*[20] have been able to grow at 850 °C highly resistive GaN films with carrier concentrations $<10^{14}/cm^3$ and mobilities as high as 200 $cm^2/V\,s$. The reduction of the background carrier concentrations to these levels has additionally allowed Kim *et al.*[20] and Yang, Li, and Wang[18] to achieve *p*-type Mg doping of GaN without post-growth annealing. The ability to achieve *n*- and *p*-type doping has allowed Grandjean *et al.*[24] to fabricate UV GaN light emitting diodes by this technique.

a)Author to whom correspondence should be addressed; electronic mail: Robert_Davis@ncsu.edu

Improvements in the characteristics of the nitride films and an increased understanding of the associated OMVPE and PAMBE growth techniques were aided by several studies[8–17] regarding the growth mechanisms of GaN and AlN on various substrates. Similar improvements in NH_3–GSMBE-derived films should also be aided by such studies. As such, the authors have employed several analytical techniques to investigate the initial growth mechanisms of GaN on AlN and AlN on GaN by the NH_3–GSMBE technique. We show that at low growth/substrate (sub) temperatures ($T_{sub}<800\,°C$), GaN growth on AlN proceeds via a layer-by-layer plus island, i.e., a Stranski–Krastanov (SK) growth mechanism. At higher temperatures ($T_{sub}>800\,°C$) it proceeds via a Frank van der Merwe (FM) layer-by-layer mechanism. No Volmer–Weber (VW) island growth was observed. Throughout the temperature range investigated, AlN was observed to grow on GaN in a FM/layer-by-layer mechanism. Based on simulations of NH_3 and H desorption, the change in the GaN growth mechanism from SK to FM is attributed to a transition from a fully ammonia/hydrogen-terminated GaN surface to a partially hydrogen-terminated surface with increasing temperature

II. EXPERIMENTAL PROCEDURE

A. Thin film growth and analysis system

All experiments described later were conducted using a unique ultrahigh vacuum (UHV) configuration which integrated several completely independent UHV thin film growth and analysis systems via a 36 ft long transfer line having a base pressure of 9×10^{-10} Torr (see Ref. 31 for details of the transfer line and many of the associated systems). The experiments described in this paper employed the III–N GSMBE, Auger electron spectroscopy (AES), low-energy electron diffraction (LEED), and x-ray photoelectron spectroscopy (XPS) systems.

1. GSMBE

The GSMBE system, with a base pressure of 3×10^{-10} Torr, was designed and constructed specifically for the growth of III–V nitride thin films. The sample heating stage consisted of a wound tungsten heating filament positioned close to the back of the sample and mounted on a boron nitride disk supported by four alumina tubes connected to the bottom of a cup-shaped molybdenum sample holder.[31] A W/6%Re–W/26%Re thermocouple was employed to measure the temperature of the backside of the wafer; heating profiles were controlled using a programmable microprocessor and 20 amp semiconductor current rectifier (SCR) power supply. Actual surface/sample temperatures (i.e., those reported herein) were measured using an infrared thermometer with a spectral response of 0.8–1.1 μm and a emissivity setting of 0.5. The estimated experimental accuracy for the latter temperatures was estimated to be $\pm25\,°C$. Surface temperatures to 1100 °C were easily obtained.

Source materials in the GSMBE included Al, Ga, and NH_3. Aluminum (99.9999%) was evaporated from a 25 cm^3 ''cold lip'' Knudsen cell, and Ga (99.99999%) was evaporated from a 25 cm^3 dual filament Knudsen cell. The NH_3 (99.9995%) was further purified via an inline metalorganic resin purifier connected directly to a leak valve mounted on the GSMBE chamber. Sample exposure to the NH_3 was obtained using ''molecular beam'' dosers similar in design to those employed by Bozack *et al.*[32] Collimation of the ammonia into a molecular beam focused onto the sample was achieved with this doser using a 13 mm diameter×2-mm-thick glass capillary array with a 10 μm pore size (Galileo Electro Optics, Inc.). The doser-to-sample distance was fixed at 5.1 cm. This doser arrangement enhanced the ammonia flux to the sample by a factor of 10–100. Residual gas analysis of the NH_3 revealed extraneous peaks at 28 and 44 indicating that CO, N_2, and CO_2 were the principal contaminants in the gas.

2. XPS System

Experiments involving XPS were performed in a stainless steel UHV chamber (base pressure $=2\times10^{-10}$ Torr) equipped with a dual anode (Mg/Al) x-ray source and a 100 mm hemispherical electron energy analyzer (VG CLAM II). All XPS spectra reported herein were obtained at 12 kV and 20 mA emission current using Mg $K\alpha$ radiation ($h\nu=1253.6$ eV). An XPS analysis typically required less than 1 h during which time the pressure never increased above 9×10^{-10} Torr. Calibration of the binding energy scale for all scans was achieved by periodically taking scans of the Au $4f_{7/2}$ and Cu $2p_{3/2}$ peaks from standards and correcting for the discrepancies in the measured and known values of these two peaks (83.98 and 932.67 eV, respectively).[33] A combined Gaussian–Lorentzian curve shape with a linear background was found to best represent the data.

3. AES/LEED

The AES and the LEED optics were mounted on a six-way cross connected to the transfer line and pumped through the transfer line. A 3 keV, 1 mA beam was used in the AES analysis. Each spectrum was collected in the undifferentiated mode and numerically differentiated. An 80 eV, 1 mA beam was used in the LEED studies.

B. Substrates and thin film preparation

The substrates used in this research were ≈1.5×1.5 cm pieces cut from 3 cm diameter off-axis (4° toward $(11\bar{2}0)$) *n*-type ($N_d=10^{18}\,cm^3$) $(0001)_{Si}$ 6H-SiC wafers obtained from Cree Research, Inc. All wafers were received with an ≈1 μm *n*-type epitaxial layer ($N_d=5\times10^{17}$) on which was grown ≈500–1000 Å of thermal oxide the generation of which was necessary in order to obtain a stoichiometric SiC surface after removal via a 10 min 10:1 HF dip.[34] The unpolished backside of each wafer was subsequently coated via rf sputtering with tungsten to increase the heating efficiency of the SiC as the latter was partially transparent to the infrared radiation emitted from the tungsten filament heater. All wafers were then ultrasonically rinsed in acetone and methanol, exposed to the vapor from a 10:1 buffered HF solution for 10 min, and mounted using Ta wire to a 1 in. diameter Mo disk with an approximately 1.5 cm^2 square hole cut in the center. Each wafer/Mo assembly was then fastened to a

ring-shaped Mo sample holder using Ta wire and inserted into the transfer line load lock. The *in situ* procedure used for the final cleaning step of the 6H-SiC substrates was similar to that described by Kaplan[35] and Kern and Davis[36] and is described in detail elsewhere.[37] Briefly, each SiC wafer was annealed in the GSMBE system in a flux of 10^{-5}–10^{-6} Torr SiH_4 for ≈15–20 min at 950–1050 °C. Analysis via AES and XPS revealed oxygen-free, silicon-terminated SiC surfaces which displayed either (1×1) or (3×3) LEED pattern. If a (3×3) LEED pattern, indicative of the formation of a bilayer of free silicon on the surface, was obtained, the sample was annealed in UHV at 1050 °C for 5–10 min to desorb the excess silicon.[37] This procedure resulted in a (1×1) pattern. Growth of the AlN buffer layer was always initiated on an oxygen-free (1×1) 6H-SiC (0001) surface.

To initiate the deposition of AlN, the 6H-SiC wafer was raised to a temperature of 1050 °C at which point the shutter to the Al Kcell (at 1150 °C) was opened. A few seconds later, ammonia was admitted into the system which created a total pressure of $\approx 10^{-5}$ Torr. Growth proceeded at a rate of 1000 Å/h for approximately 15 min after which the Al cell was shuttered. The sample was cooled in flowing ammonia until approximately 800–900 °C at which point the ammonia valve was closed. The AlN films displayed (2×2) reconstructed surfaces in LEED immediately after growth and cooling to about 100–200 °C. This reconstruction was sensitive to contamination or temperature, as a (1×1) LEED pattern was observed several hours after growth when the sample had reached room temperature. Observations via scanning electron microscopy (SEM) at 10 000× magnification showed the films to be free of surface topography. The films were too resistive for electrical measurements. Additional details regarding this research have been published elsewhere.[38–40]

To achieve the growth of each GaN film on an AlN buffer layer, the latter was heated to 650–800 °C in 10^{-4} Torr ammonia (50 sccm) after which the Ga cell (at 1020 °C) was opened and growth allowed to proceed. The growth rate for these conditions was determined via cross-sectional SEM to be ≈ 2000 Å/h. After the desired GaN thickness had been achieved, the Ga cell was closed. Each film was allowed to cool in flowing ammonia to approximately 600 °C after which the valve for this gas was closed.

Films of AlN were also deposited at 800 °C and 10^{-5} Torr NH_3 on undoped (0001) GaN films previously grown by both GSMBE in the authors' system and OMVPE. The other process parameters were similar to those used in the growth of the AlN buffer layers. The OMVPE GaN films were cleaned by annealing in 10^{-4} Torr NH_3 at 900 °C for 15 min. AES and XPS did not detect the presence of oxygen or carbon.[41]

C. Growth mode analysis

The experimental procedure and analysis used to study the growth modes of GaN (AlN) on AlN (GaN) were similar to that used by Sitar, Smith, and Davis[17] to study the growth modes of AlN and GaN on $(0001)_{Si}$ 6H-SiC and (0001) Al_2O_3. Therefore, only a brief description of the procedure will be given here.

A series of sequential depositions, each having a thickness of ≈0.5–5 Å of GaN (AlN) on AlN (GaN), were conducted until a GaN (AlN) film thickness of ≈35 Å was achieved. Following each deposition, XPS, LEED, and AES analysis were performed. Each series of depositions and analysis was completed within 12–14 h to ensure the cleanliness of the surfaces and interfaces. To determine the growth mode of the GaN (AlN) film, the ratio of the initial integrated intensity, I_0, of the Al $2p$ (Ga $3p$) core level from the AlN buffer layer (OMVPE GaN film) was measured against the integrated intensity, I_S, of the Al $2p$ (Ga $3p$) core level from the GaN/AlN interface. The values of I_s/I_0 were plotted against the calculated GaN thickness (=growth rate ×growth time). Theoretical curves for the Al $2p$ (Ga $3p$) attenuation expected from FM, SK, and VW growth modes were simultaneously plotted and compared with the experimentally determined attenuation to elucidate the growth mode(s). The following relations were used for the three modes:

FM

$$I_s/I_0 = \exp(-t/\lambda), \tag{1}$$

where t = thickness of the growing film, λ = mean free path of the photoelectron being measured, I_0 = initial intensity of the substrate core level, and I_s = intensity of the substrate core level with a overlying film of thickness t.

SK

$$I_s/I_0 = (1-\theta) + \theta \exp(-t/\lambda), \tag{2}$$

where θ is the surface coverage of the film/islands.

VW

$$I_s/I_0 = (1-\theta)\exp(-q/\lambda) + \theta \exp(-t/\lambda), \tag{3}$$

where q = thickness of the film before onset of 3D growth.

The following relation from Briggs and Seah[33] was used to calculate the mean free paths of the core levels of interest

$$= 0.41(aE)^{1/2} + 538E^{-2} \text{ monolayers}, \tag{4}$$

where E = kinetic energy of the photoelectron, $a = (\rho M_W / N_A)^{1/3}$ where, ρ = density of overlying film, M_W = molecular weight of film, N_A = Avogadro's Number.

The mean free path of Al $2p$ photoelectrons in GaN was determined to be 19 Å. The mean free paths of Ga, $3d$, $3p$, and $2p$ photoelectrons in AlN were determined to be 19, 18, and 6 Å, respectively.

III. RESULTS

A. Growth of GaN films on AlN

Figure 1 shows a plot of the attenuation of the Al $2p$ core level as a function of the thickness of the overlying GaN films grown at 650 °C. Curves for the expected attenuation for FM, SK, and VW growth modes are also included. The Al $2p$ core level intensity increased after the first few GaN depositions. This phenomenon is believed to be due to forward scattering effects wherein the trajectory of a photoelec-

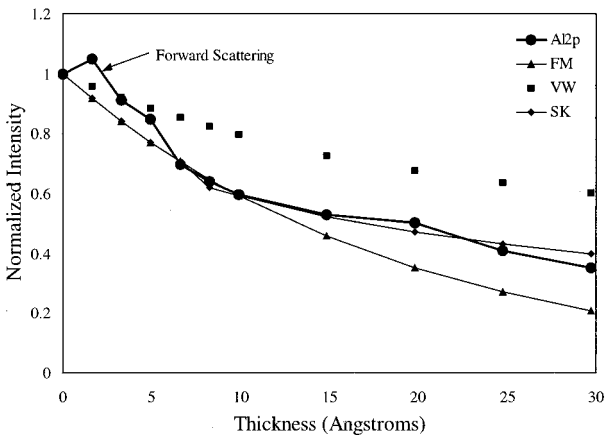

FIG. 1. Attenuation of the Al $2p$ core level from the AlN buffer layer as a function of overlying GaN film thickness for $T_{sub}=650\,^{\circ}\mathrm{C}$. Circles =experimental I/I_0, triangles=theoretical I/I_0 for FM layer-by-layer growth, squares=theoretical I/I_0 for VW growth, diamonds=theoretical I/I_0 for SK growth.

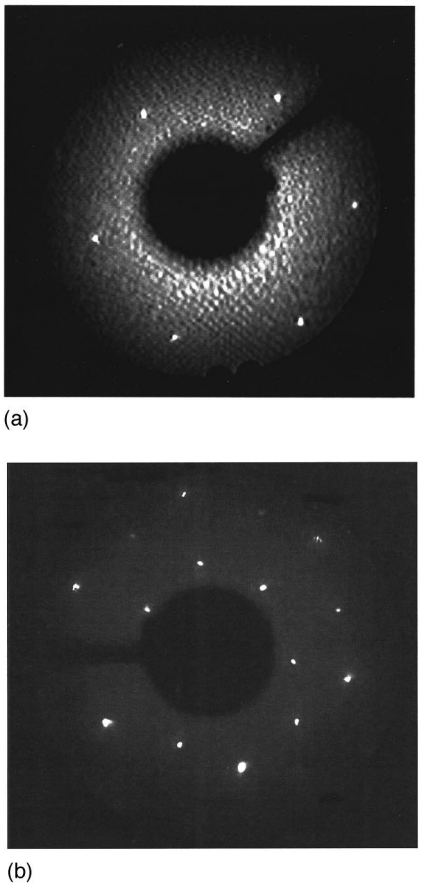

FIG. 2. LEED patterns from (a) (1×1) (0001) GaN, and (b) (2×2) (0001) GaN films deposited on AlN(0001) at 650 and 800 °C, respectively.

tron emitted by an underlying atom is bent in the direction of the overlying atom due to the positive charge of the nucleus of the latter.[42,43] This can cause an increase in the intensity of the core levels along certain crystallographic directions.[42] This effect diminished with further depositions, and the subsequent data followed a curve which most closely matched that expected for FM growth. However, at a GaN thickness of 15 Å, the Al $2p$ attenuation again exhibited an increasingly positive deviation from the curve for FM growth and approached the curves expected for SK and VW growth. An excellent fit to the experimental data was obtained by assuming SK growth with a 2D growth thickness of 10 Å.

Unreconstructed (1×1) LEED patterns representative of those displayed throughout the entire sequence of GaN depositions described above are shown in Fig. 2(a). The oxygen levels measured by AES and XPS throughout the series were either undetectable or less than 1% of a monolayer. The representative microstructure of the surface of the GaN films grown at 650 °C is shown in Fig. 3(a) for film thicknesses of 4–5000 Å. These films were *n* type and extremely conductive. Four point probe (4pp) measurements showed sheet resistances of $10^{-2}\,\Omega$/sq, indicative of free carrier concentrations of $10^{19}/\mathrm{cm}^3$.[44] Photoluminescence spectra of these films showed very broad donor bound exciton emission of weak intensity as shown in Fig. 4(a).

Figure 5 shows a plot of the Al $2p$ attenuation as a function of GaN thickness for films grown on AlN at 800 °C. As for the films grown at 650 °C, the Al $2p$ intensity increased after the first few GaN depositions and then decreased to match the curve expected for FM growth. However, unlike GaN growth at 650 °C, the Al $2p$ attenuation continued to follow the curve expected for FM growth until the Al $2p$ was essentially undetectable. The SEM micrograph in Fig. 3(b) shows a very smooth surface containing occasional ''pits'' similar in appearance to those observed in thin OMVPE GaN surfaces suggesting that layer-by-layer growth was maintained at thicknesses greater than that sampled by XPS. The rms surface roughness of this film as determined by atomic force microscopy was approximately 40 Å, which is comparable to the <20 Å typically measured from high-quality OMVPE GaN surfaces.

Reconstructed (2×2) LEED patterns were displayed throughout the series of GaN depositions on AlN at 800 °C [see Fig. 2(b)]. These surfaces were similarly sensitive to surface contamination and temperature as the (2×2) reconstructed AlN surface. Typically, (1×1) LEED patterns developed after 3–4 h in a vacuum of 10^{-9}–10^{-8} Torr. The (2×2) reconstructed surfaces could be restored by annealing in 10^{-5} Torr NH_3 for 5 min. No attempts were made to determine the actual structure of the (2×2) reconstruction. However, the theoretical work of Rapcewicz, Nardelli, and Bernholc[45] indicates that a (2×2) N adatom reconstruction is energetically most favorable for Ga terminated (0001) GaN, and a (2×2) N vacancy reconstruction is energetically favorable for the nitrogen-terminated (0001) GaN surface. The oxygen levels detected by both AES and XPS from the GaN films grown at 800 °C were similarly found to be undetectable (i.e., <1%).

The GaN films grown at 800 °C were more resistive (0.2–1 M Ω) than those grown at 650 °C. Sheet resistances for the former were typically too high for 4pp measurements. The carrier concentrations (N_D-N_A) of the 800 °C films determined by capacitance voltage (CV) measurements were in the range of $1-5\times10^{17}/\mathrm{cm}^3$. Films grown at 825 °C were more resistive with a carrier concentration of 2–5

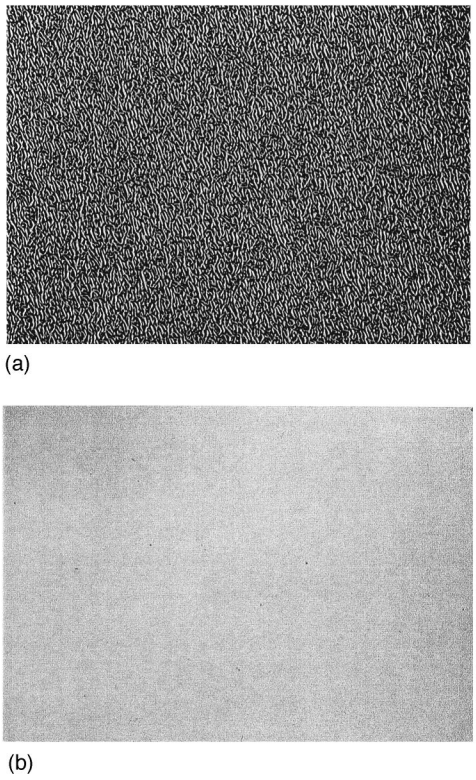

FIG. 3. SEM micrographs of GaN films grown on AlN buffer layer at (a) 650 and (b) 800 °C.

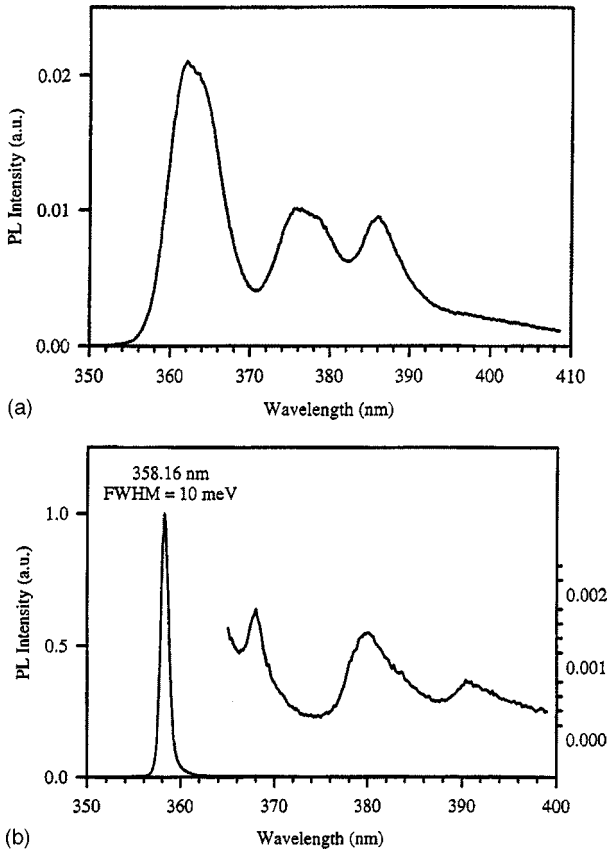

FIG. 4. Photoluminescence of GaN films grown on AlN buffer layer at (a) 650 and (b) 800 °C.

$\times 10^{16}/\mathrm{cm}^3$. However, Hall measurements found $n=2\times 10^{17}/\mathrm{cm}^3$ and $\mu=60\ \mathrm{cm}^2/\mathrm{V\,s}$. Photoluminescence of these films displayed sharp [full width at half maximum=10 meV] donor-bound exciton emission and very little $D-A$ emission, see Fig. 4(b).

B. Growth of AlN films on GaN

A plot of the attenuation of the Ga $3p$ core level from an OMVPE GaN film as a function of overlying AlN thickness is shown in Fig. 6. 2D (FM) growth of the AlN films on the OMVPE GaN was observed to occur. Similar results were obtained for AlN growth on GSMBE GaN. No surface topography was observed on the AlN surface via SEM, but the AlN/GaN was observed to have cracked. The cause of the cracking is currently not known. The resistivity of these AlN films were beyond the range of our experimental capabilities, and CV did not indicate any charge.

IV. DISCUSSION

A. Strain effects

The results of the XPS CL attenuation research shown in Figs. 1 and 5 clearly indicate that the growth of GaN on monocrystalline AlN by NH_3–GSMBE initially proceeds in a FM/layer-by-layer mechanism between 650 and 800 °C. We have further observed, using XPS in tandem with SEM, that growth can either continue in a FM/layer-by-layer mode or switch to a 3D SK growth regime depending on the growth temperature. Further inspection of Fig. 1 reveals that the deviation from the expected Al $2p$ attenuation for FM growth and the experimentally observed Al $2p$ attenuation occurs at ≈10–15 Å which is also the reported Matthews–Blakeslee critical thickness for GaN on AlN.[46] This observation is clearly in line with the classical interpretation of SK type growth where growth starts in a 2D fashion and then the buildup of interfacial stress forces 3D growth. However, the thickness of the underlying 250 Å monocrystalline AlN buffer layer exceeds the critical thickness for AlN on 6H-SiC (≈46 Å[47]) and is highly defective with a large density of

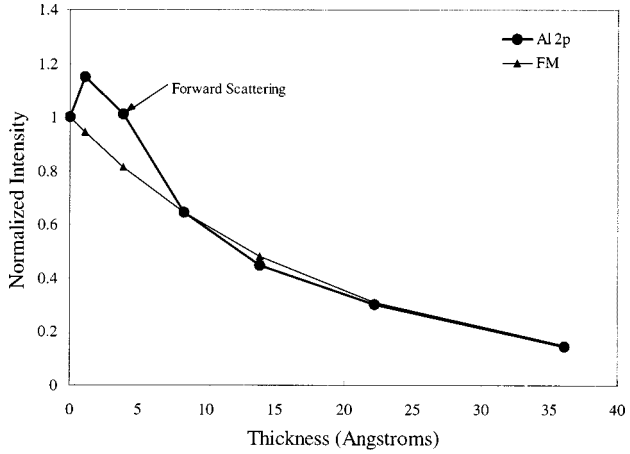

FIG. 5. Attenuation of Al $2p$ core level from AlN buffer layer as a function of overlying GaN film thickness for $T_{\mathrm{sub}}=800$ °C. Circles=experimental I/I_0, triangles=theoretical I/I_0 for FM layer-by-layer growth.

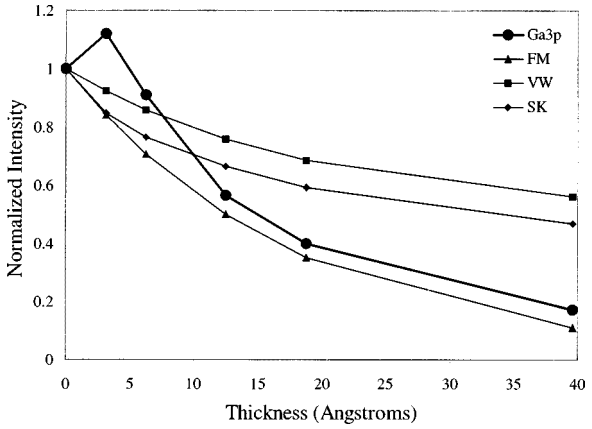

FIG. 6. Attenuation of Ga $3p$ core level from OMVPE GaN film as a function of overlying AlN film thickness for $T_{sub}=800\,^{\circ}C$. Circles =experimental I/I_0 for Ga $3p$, triangles=theoretical I/I_0 for FM layer-by-layer growth, squares=theoretical I/I_0 for VW, diamonds=theoretical I/I_0 for SK growth.

misfit dislocations of which a substantial portion propagate into the GaN film.[47–50] Accordingly, there already exists a high density of defects at the GaN/AlN interface which can act as low energy nucleation sites for misfit dislocations.

To further argue against interfacial strain causing the change in growth mode, it is worth noting that a switch from a 3D to a 2D growth mode with substrate temperature has also been observed using RHEED by Powell, Lee, and Greene[30] for growth of GaN directly on (0001) Al_2O_3 via NH_3–GSMBE. These RHEED studies showed that films grown at (i) $T_{sub}<760\,^{\circ}C$ exhibited well-defined transmission spots indicative of 3D island growth and at (ii) $T_{sub}>780\,^{\circ}C$ exhibited sharp Kikuchi lines and streaky (1×1) patterns indicative of 2D growth. As the lattice matching and interfacial bonding between GaN and Al_2O_3 are completely different from that of GaN on AlN, one would not expect to see a switch from 3D to 2D growth in the same temperature range if strain relaxation mechanisms were responsible for the changes in growth mechanism.

B. Surface effects

Simultaneous to the change in growth mode from 3D to 2D, a change in surface structure from an unreconstructed (1×1) surface at $T_{sub}<800\,^{\circ}C$ to a reconstructed (2×2) surface at $T_{sub}>800\,^{\circ}C$ was observed with LEED. The observed improvement in the electrical and optical properties in GaN films grown at 800 °C with the change in growth mode and surface structure suggests that a more optimized growth regime was perhaps realized. Further, the concomitant change in growth mode and electrical/optical properties with surface order and temperature suggests that the change in growth mode may be related to a change in the kinetics of one of the surface-limiting processes (i.e., adsorption, desorption, diffusion, etc.). Accordingly, it is important to note that for all temperatures investigated, no Ga accumulation (i.e., Ga droplets) was observed to occur as evidenced by the lack of any metallic Ga $3d$, $3p$, or $2p$ features in XPS. In addition, based on the isothermal growth phase diagram of Jenny, Kaspi, and Evans,[51] only GaN growth should be expected for the process parameters examined. Therefore, the 3D/2D transition should not be due to a transition from Ga accumulation to desorption.

A similar $3D\rightarrow2D/(1\times1)\rightarrow(2\times2)$ transition has also been observed in PAMBE growth of GaN on various different substrates and buffer layers.[15,52] In PAMBE, a transition from a (1×1) to (2×2) RHEED pattern and a transition from 3D to 2D growth has been reported when the growth temperature is increased beyond a certain point. Similarly, an improvement in structural, electrical, and optical properties has also been observed. In the case of PAMBE, the transition from 3D to 2D growth and a (1×1) unreconstructed surface to a (2×2) reconstructed surface was concluded to occur when moving from a N rich/stabilized surface to a Ga rich/stabilized surface.[15] Recently, Held *et al.* have used desorption mass spectroscopy (DMS) and RHEED to study NH_3–GSMBE growth of GaN and have also observed two distinct growth regimes which they classified as NH_3 and Ga limited growth.[53] In NH_3 limited growth, weak (2×2) reconstructed RHEED patterns and smooth surfaces were observed, whereas for Ga limited growth, transmission RHEED patterns indicative of 3D growth were observed.

The observations of Ga limited/N rich-stabilized surfaces for 3D GaN growth and NH_3 limited/Ga-rich stabilized surfaces in 2D GaN growth for both NH_3–GSMBE and PAMBE, respectively, supports the conclusion that surface processes/kinetics are responsible for the observed $3D\rightarrow2D$ transition. However, a detailed understanding of the particular surface process influencing the growth mechanism is still lacking. Of further concern is the difference in temperature at which the transition from $(1\times1)\rightarrow(2\times2)$ and $3D\rightarrow2D$ is observed to occur in PAMBE and NH_3–GSMBE. In PAMBE, the transition is observed to occur at temperatures of 600–675 °C, whereas in NH_3–GSMBE it is observed to occur at 750–800 °C which is 100–200 °C higher.[15,30,40,52] Also of concern, is the observation of an NH_3-limited GaN growth regime in NH_3–GSMBE in cases where the NH_3/Ga ratio is >10–100.

At this point, it is worth noting that a similar phenomena has been observed in Si and Ge homoepitaxial MBE where the transition temperature from 3D to 2D growth for GS, MBE using SiH_4, Si_2H_6, or GeH_4 is observed to occur at 100–200 °C higher temperature than that which is observed to occur for solid source MBE of these materials.[54–56] The transition from 3D to 2D growth has been proposed to be due to slow hydrogen desorption kinetics from Si which results in sight blocking of surface adsorption sites at low growth temperatures.[56] This theory has been supported by the experiments of Sakamoto *et al.*[55] which showed that the addition of atomic hydrogen to the solid source growth of Si in a 2D growth regime forced growth to occur in 3D fashion. This suggests that surface processes such as adsorption/desorption of hydrogen and or decomposition of ammonia on GaN surfaces could also be the reason for the higher 3D–2D transition temperature in NH_3–GSMBE relative to PAMBE. To further support this argument, the authors note that Yu *et al.*[57] have observed that the addition of atomic H to the PAMBE growth of GaN in a regime where 2D growth is typically observed can cause growth to switch to 3D. As

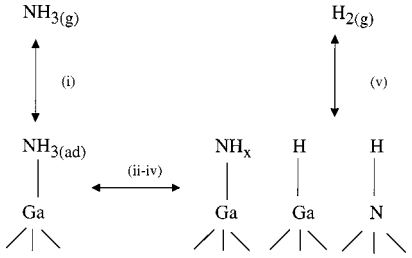

FIG. 7. Schematic illustrating the interaction of ammonia (NH_3) with a GaN surface.

noted by Tarsa *et al.*,[15] the transition from 3D→2D growth in PAMBE could be due to limited Ga adatom surface mobility due to the presence of three nitrogen dangling bonds. If these dangling bonds are instead capped with hydrogen atoms, it could further act to reduce the Ga adatom mobility, as well as limit the incorporation of Ga.

We provide a simple model for the interaction of NH_3 with GaN surfaces in MBE which shows that hydrogen desorption/ammonia decomposition may be the determining factor for the NH_3–GSMBE GaN growth mechanism. This model will further explain the observation of NH_3/Ga limited growth regimes for conditions in which NH_3/Ga $>10-100$.

C. Ammonia/hydrogen desorption

Based on the residual gas analyzer studies of Kamp *et al.*[21] for the surface cracking of ammonia on GaN, and the temperature programmed desorption (TPD) high-resolution electron energy-loss spectra/electron stimulated desorption ion angular distribution studies of the adsorption/desorption of NH_3 on Si (111)[58,59] and NH_3 on GaAs (100),[60] we propose the following sequences of reactions for describing the reaction of ammonia with GaN surfaces

$$NH_{3g} \Leftrightarrow NH_{3ad} \quad \text{(i)}$$

$$NH_{3ad} \Leftrightarrow NH_{2ad} + H_{ad} \quad \text{(ii)}$$

$$NH_{2ad} + H_{ad} \Leftrightarrow NH_{ad} + 2H_{ad} \quad \text{(iii)}$$

$$NH_{ad} + 2H_{ad} \Leftrightarrow N_{ad} + 3H_{ad} \quad \text{(iv)}$$

$$2H_{ad} \Leftrightarrow H_{2g} \quad \text{(v)}$$

$$2N_{ad} \Leftrightarrow N_{2ad} \Leftrightarrow N_{2g} \quad \text{(vi) No growth}$$

$$Ga_{ad} + N_{ad} \Leftrightarrow GaN_s \quad \text{(vii) GaN growth.}$$

As shown in Fig. 7, the GaN growth direction is assumed to occur in the [0001] direction with a Ga-terminated surface being maintained. This is based on the fact that growth of the AlN buffer layer was initiated on a silicon terminated $(0001)_{Si}$ 6H-SiC surface and that a C–Si–N–Al interface is subsequently expected. Maintaining the same polarity across the AlN/GaN interface would lead to a Ga-terminated surface. In Fig. 7, it should also be noted that the initial adsorption of ammonia is assumed to occur molecularly and explicitly at Ga surface sites. Based on the results of Dresser *et al.*[58] and Tanaka, Onchi, and Nishijima[59] from studies of NH_3 adsorption onto Si (111), some dissociative adsorption of ammonia is also assumed to occur with NH_{xad} and H_{ad} being formed. However, no site specificity (N or Ga) is assigned to the H_{ad}.

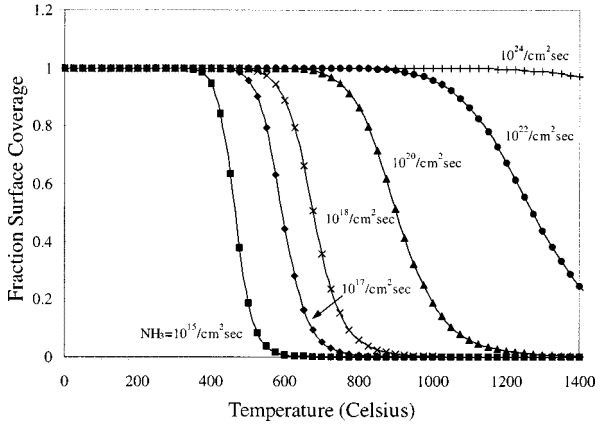

FIG. 8. Ammonia surface coverage as a function of temperature and ammonia flux.

For simplicity, we will start by modeling the reactions (i) (i.e., ammonia adsorption and desorption) followed by reaction (v), i.e., adsorption and desorption of hydrogen from GaN surfaces. Our approach is to estimate the steady-state surface coverage of ammonia or hydrogen on GaN and AlN surfaces in the presence of a flux of NH_3. This will allow the ammonia/hydrogen surface coverage during NH_3–GSMBE growth to be estimated and accordingly determine the temperature at which ammonia desorption and/or decomposition on GaN and AlN surfaces is rapid and not the limiting reaction.

Desorption kinetics are typically described by the general Polyani–Wigner expression[61]

$$\text{desorption rate} = -d\theta/dt = \nu_n \theta^n \exp(-E_{\text{des}}/RT), \quad (5)$$

where n=the reaction order, θ=the adsorbate surface coverage, ν=the pre-exponential factor ($\nu_0 = 10^{28}\,\text{cm}^2\,\text{s}$, $\nu_1 = 10^{13}/\text{s}$, $\nu_2 = 10^{-2}\,\text{cm}^2/\text{s}$), and E_{des}=the activation energy for desorption. In steady-state conditions, the flux of adsorbates leaving the surface via desorption will be equal to the incoming flux of the adsorbate times the adsorbate sticking coefficient. The sticking coefficient (S) is described by

$$S = S_0(1 - \theta/\theta_{\max})^n, \quad (6)$$

where S_0=the initial sticking coefficient (at $\theta=0$) and is assumed equal to unity in the analysis, and $\theta_{\max}$ is the maximum surface coverage ($\approx 2.3\times 10^{15}$ atoms/cm^2). The combination of Eqs. (5) and (6) allows the determination of the steady-state surface coverage of the adsorbate.[62]

Based on a Redhead analysis of TPD spectra from the desorption of ammonia from Si (111) surfaces, Dresser *et al.*[58] determined that molecular desorption of NH_3 from this surface was first order and estimated that $E_{\text{des}} = 46$ kcal/mol assuming $\nu_1 = 10^{14}/\text{s}$. As illustrated in Fig. 8, these parameters were used to generate a plot of ammonia surface coverage versus temperature for various different ammonia fluxes. Figure 8 clearly shows that for Si (111), a fully ammonia-saturated surface would be maintained up to temperatures of 600 °C. Due to the increased electron sharing

between the electron deficient Ga surface atom and the unbonded electron pair on the NH_3 molecule, it is reasonable to expect that the Ga–NH_3 bond is stronger than the Si–NH_x. This could lead to a higher E_{des} for NH_3 from GaN and thus, push the equilibrium NH_3 saturation surface coverage shown in Fig. 8 to higher temperatures. However, the important feature to clarify here is that if NH_3 adsorption is predominantly molecular, decomposition of adsorbed NH_3 species to NH_x (reactions ii–iv) will be prohibited due to saturation of all surface sites with NH_3, as well as possible steric hindrance effects. Thus temperatures >700 °C are needed to provide open surface sites for dissociation of adsorbed NH_3 species into NH_x and H_{ad}.

Desorption of hydrogen on GaN may occur from both Ga and N sites. Chiang *et al.*[63] using isothermal analysis and direct recoil time-of-flight mass spectroscopy have recently determined that deuterium desorption from Ga sites on Ar^+ sputter cleaned polycrystalline GaN surfaces is second order with an activation energy of 9 kcal/mol. The findings of these authors for H desorption from Ga are similar to those for hydrogen desorption from Ga in GaAs where a second order desorption activation energy of 13 kcal/mol was determined.[64] Second order desorption is consistent with the following recombinative desorption mechanism

$$2D_{ads} \rightarrow GaD_2 \rightarrow D_{2(g)} + Ga. \quad (7)$$

Chiang *et al.* speculate that the rate limiting reaction in this expression is actually diffusion of the deuterium to Ga sites and that D_2 desorption is rapid. Unfortunately, Chiang *et al.* did not provide information regarding hydrogen desorption from nitrogen sites except that it is complete by 600 °C. This is supported by the ammonia and deuterium TPD studies of Shekhar and Jensen[65] on N_2 sputter-cleaned OMVPE GaN films grown on Al_2O_3. Their TPD studies showed a peak in D_2 desorption at ≈500 °C for low surface coverage's which shifted to 350–400 °C with saturated surface coverage's indicative of second order desorption kinetics. However, their TPD studies were not successful in determining whether the desorption was from Ga or N sites. The presence of incompletely dissociated NH_x at temperatures of >750 °C is supported by the DMS studies of Held *et al.*[53] which observed the evolution of hydrogen when ammonia saturated surfaces were exposed to Ga at this temperature. Further support for N–H bonding on GaN/AlN surfaces at higher temperatures is provided by Fourier-transform infrared studies of the interaction of NH_3 and trimethyl aluminum on AlN/Al_2O_3 surfaces by Liu, Bertolet, and Rogers[66] and the soft x-ray photoemission spectroscopy studies of the adsorption of NH_3 on SiC, $LiGaO_2$, and GaN by Klauser, Kumar, and Chuang.[67]

Based on the earlier observations, we have estimated that hydrogen desorption from nitrogen surface sites on GaN is second order with an activation energy of 55 kcal/mol. This estimation is based on the similar bond energies of hydrogen to nitrogen and silicon in ammonia and silane (431.8 and 393.3 kJ/mol, respectively)[68] and the determination of second order desorption kinetics of hydrogen from Si (111) with $E_{des}=57.5$ kcal/mol by Schulze and Henzler.[69] There have been no reports on E_{des} for hydrogen specifically from a nitrogen site on a nitride surface to support this assumption. However, hydrogen desorption sites from polycrystalline MoN with $E_{des} \cong 50$ kcal/mol have been reported by Choi, Lee, and Thompson.[70] For hydrogen desorption from AlN, we considered hydrogen desorption from nitrogen sites in AlN to be similar to hydrogen desorption from nitrogen sites on GaN surfaces, and hence, assumed $E_{des}=55$ kcal/mol. For hydrogen desorption from Al sites on AlN, we used the experimentally determined activation energies of hydrogen desorption from metallic (111) Al surfaces which are 17 kcal/mol for zeroeth order desorption kinetics.[71] An activation energy of 17 kcal/mol and second order desorption kinetics were assumed in the calculations described herein.

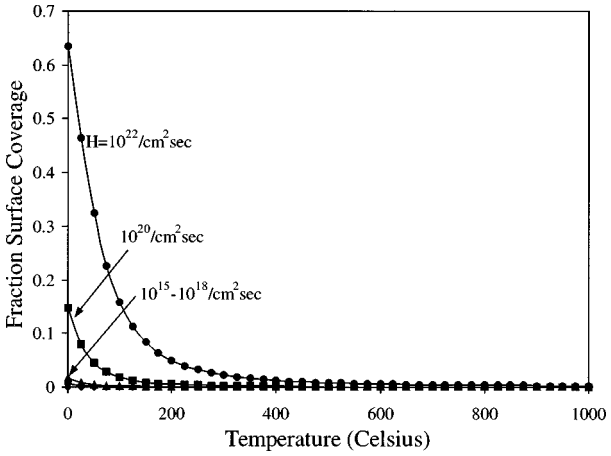

FIG. 9. Hydrogen surface coverage on Ga sites of (0001) GaN as a function of temperature and atomic H flux (#/cm^2 s).

Using $E_{des}(H_{Ga})=9$ kcal/mol, $E_{des}(H_{Al})=17$ kcal/mol, $E_{des}(H_N)=55$ kcal/mol, $\nu_2=10^{-2}$ cm^2/s, $S_0=1$ and $\theta_{max}=2.3\times10^{15}/cm^2$, plots of hydrogen surface coverage on Ga, Al, and N sites of GaN or AlN surfaces were generated as a function of temperature for various ammonia fluxes (see Figs. 9–11). As can be seen in Fig. 9, very little hydrogen remains adsorbed to Ga at any temperature except for extremely large fluxes of ammonia ($10^{24}/cm^2$ s). However, for ammonia fluxes of $10^{17}-10^{18}/cm^2$ s (i.e., typical NH_3–MBE

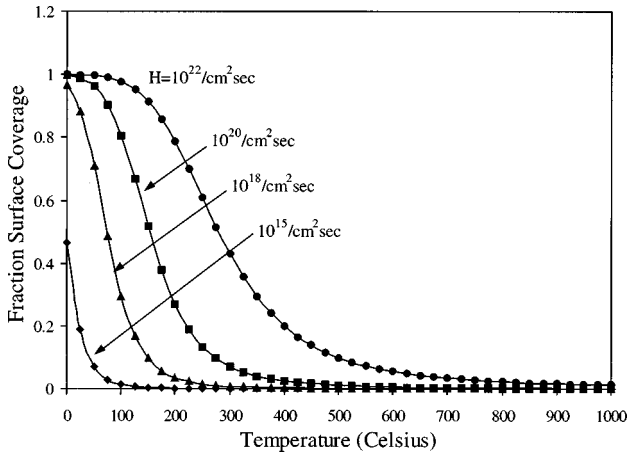

FIG. 10. Hydrogen surface coverage on Al sites of (0001) AlN as a function of temperature and atomic H flux (#/cm^2 s).

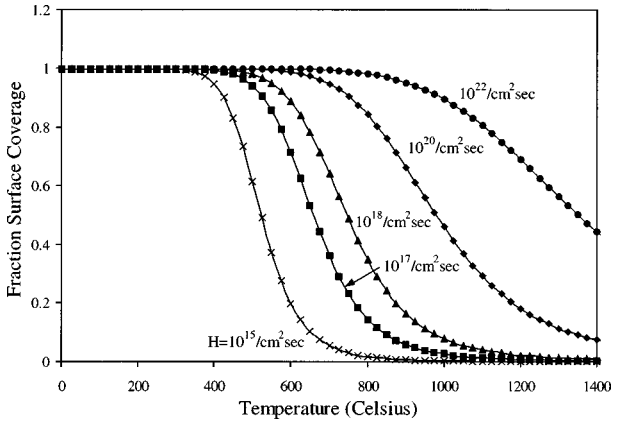

FIG. 11. Hydrogen surface coverage on N sites of (0001) GaN and/or AlN as a function of temperature and atomic H flux (#/cm^2 s).

conditions) hydrogen is stable on Al sites on AlN surfaces to temperatures of 100 °C, see Fig. 10. In contrast, Fig. 11 shows that saturation of nitrogen sites with hydrogen is observed to occur for all fluxes to temperatures of 550 °C. Figure 11 also shows that desorption of hydrogen from nitrogen sites is nearly complete at 600 °C for low ammonia fluxes, which is consistent with the observations of Chiang *et al.*[63] and Shekhar and Jensen[65] and lends support to our assumptions for the activation energy for desorption of hydrogen from nitrogen. Further inspection of Fig. 11 reveals that for ammonia fluxes of $10^{17}-10^{18}$/cm^2 s, hydrogen desorption does not become significant until temperatures of 700–800 °C. This is exactly the temperature range in which the 3D→2D transition is observed to occur for GaN growth by NH_3–GSMBE.

Based on the earlier findings, it now seems reasonable to ascribe the observed change in GaN growth from SK to FM with increasing temperature to reactive site blocking by incomplete desorption of hydrogen and or decomposition of ammonia on GaN surfaces. For typical NH_3–GSMBE fluxes and at temperatures below 700 °C, Figs. 8 and 11 show that the GaN surface is saturated with undecomposed or partially decomposed ammonia which effectively blocks reactive surface sites for NH_3 decomposition to NH_x and H_{ad}, as well as preventing incorporation of Ga into the GaN lattice. At higher temperatures ($T_{sub}>780$ °C), hydrogen desorption/ammonia decomposition is more complete leaving more open reactive sites for NH_3 dehydrogenation with which to incorporate the incoming Ga. As suggested by Chiang *et al.* and others[62,72] and as observed by the DMS results of Held *et al.*, Fig. 9 shows that adsorbed Ga atoms and Ga surface sites can act to catalyze the decomposition of NH_3 on the GaN surface via rapid desorption of hydrogen from the surface. This would explain the Ga/NH_3-limited regime observed by Held *et al.*[53] At the low temperatures where a Ga limited GaN growth regime is observed by Held *et al.*, the GaN surface is saturated by hydrogen/undecomposed ammonia and hydrogen desorption/ammonia decomposition is enhanced and accelerated by the presence of adsorbed Ga atoms. The presence of more Ga on the surface will accelerate the hydrogen desorption/ammonia decomposition kinetics and increase the growth rate. At higher temperatures, hydrogen desorption and ammonia desorption/decomposition is fast enough that only a partially hydrogen-terminated surface can be maintained. The increased desorption kinetics leads to a decreased residence time for adsorbed nitrogen species, and hence, the GaN growth rate becomes NH_3 residence time limited. Further, the lack of hydrogen on the surface can also lead to decreased surface coverage and or residence time for adsorbed nitrogen species due to increased recombinative desorption of molecular N_2.

Figure 11 shows that for higher NH_3 fluxes of $10^{20}-10^{22}$/cm^2 s characteristic of chemical vapor deposition (CVD) growth, hydrogen saturated surfaces are maintained up to temperatures of 950–1050 °C. This is the temperature range in which OMVPE growth of high-quality GaN is observed to occur. This suggests that the need for high temperatures in CVD growth of GaN is not to decompose NH_3 per se, but to increase the kinetics to the point that the surface can handle the large fluxes of species impinging on it. Further, based on comparisons between NH_3–GSMBE and PAMBE, these results indicate that the presence of hydrogen serves to stabilize nitrogen on the growing GaN surface.

D. AlN growth mechanism on (0001) GaN

As shown in Fig. 6 AlN growth on GaN is observed to occur by a layer-by-layer mechanism. This complements the research by Sitar, Smith, and Davis[17] in which it was observed that in ECR–MBE, AlN grows in a layer-by-layer fashion on both Al_2O_3 and SiC. By the same method, we have additionally observed 2D FM/layer-by-layer growth of AlN on (0001) 6H-SiC by NH_3–GSMBE. Further, the observation of 2D growth in the 750–900 °C range is consistent with our model for NH_3/H decomposition and desorption controlling the growth mode.

V. SUMMARY

XPS was used to examine the initial stages of GaN growth on AlN and AlN growth on GaN via of NH_3–GSMBE. The growth mechanism of GaN on AlN was dependent on the growth temperature; it changed from a SK-type growth to a FM-type growth with increasing temperature. A change in the surface structure and a drastic improvement in the electrical and optical properties of the resulting GaN films were observed following the change in the growth mode. At 650 °C, the transition from 2D→3D growth for a SK mechanism occurred at a film thickness of 10–15 Å. A FM/layer-by-layer type growth mechanism was observed for both GaN on AlN and AlN on GaN at temperatures >750 °C. Based on simulations of the adsorption/desorption of ammonia and hydrogen on AlN and GaN surfaces, the change in the GaN growth mechanism from SK to FM with temperature was attributed to a change from a surface saturated with ammonia and hydrogen to a partially saturated surface.

ACKNOWLEDGMENTS

The authors wish to thank Cree Research, Inc. for the 6H-SiC wafers. The research was supported by the Office of Naval Research under Contract No. N00014-92-J-1477 (M.

Yoder, Technical Monitor) and the Department of Education via an Electronic Materials/GAANN Fellowship. R. F. Davis was partially supported by a Kobe Steel, Ltd. Professorship.

[1] S. Nakamura, M. Senoh, N. Isawa, and S. Nagahama, Jpn. J. Appl. Phys., Part 2 **34**, L797 (1995).
[2] S. Nakamura, M. Senoh, S. Nagahama, N. Isawa, and T. Yamada, Jpn. J. Appl. Phys., Part 2 **35**, L74 (1996).
[3] A. Kahn, M. Shur, J. Kuznia, and Q. Chen, Appl. Phys. Lett. **66**, 1083 (1995).
[4] A. Kahn, J. Kuznia, D. Olson, W. Schaff, J. Burns, and M. Shur, Appl. Phys. Lett. **65**, 1121 (1994).
[5] S. Binari, H. Dietrich, G. Kelner, L. Rowland, K. Doverspike, and D. Gaskill, Electron. Lett. **30**, 909 (1994).
[6] H. Kong, M. Leonard, G. Bulman, G. Negley, and J. Edmond, Mater. Res. Soc. Symp. Proc. **395**, 903 (1996).
[7] Y. Wu, B. Keller, S. Kellar, D. Kapolnek, P. Kozodov, S. Denbaars, and U. Mishra, Appl. Phys. Lett. **69**, 438 (1996).
[8] H. Amano, I. Akasaki, K. Hiramatsu, N. Koide, and N. Sawaki, Thin Solid Films **163**, 415 (1988).
[9] I. Akasaki, H. Amano, Y. Koide, K. Hiramatsu, and N. Sawaki, J. Cryst. Growth **98**, 209 (1989).
[10] W. Qian, M. Skowronski, M. De Graef, K. Doverspike, L. B. Rowland, and D. K. Gaskill, Appl. Phys. Lett. **66**, 1252 (1995).
[11] K. Hiramatsu, S. Itoh, H. Amano, I. Akasaki, N. Kuwano, T. Shiraishi, and K. Oki, J. Cryst. Growth **115**, 628 (1991).
[12] N. Kuwano, T. Shiraishi, A. Koga, K. Oki, K. Hiramatsu, H. Amano, K. Itoh, and I. Akasaki, J. Cryst. Growth **115**, 281 (1991).
[13] K. Wang, D. Pavlidis, and J. Singh, J. Appl. Phys. **80**, 1823 (1996).
[14] K. Uchida, A. Watanabe, F. Yano, M. Kouguchi, T. Tanaka, and S. Minagawa, J. Appl. Phys. **79**, 3487 (1996).
[15] E. Tarsa, B. Heying, X. Wu, P. Fini, S. DenBaars, and J. Speck, J. Appl. Phys. **82**, 5472 (1997).
[16] J. Kunia, M. Kahn, and D. Olson, J. Appl. Phys. **73**, 4700 (1993).
[17] Z. Sitar, L. L. Smith, and R. F. Davis, J. Cryst. Growth **141**, 11 (1994).
[18] Z. Yang, L. K. Li, and W. I. Wang, Appl. Phys. Lett. **67**, 1686 (1995).
[19] L. K. Li, Z. Yang, and W. I. Wang, Electron. Lett. **31**, 2127 (1995).
[20] W. Kim, O. Aktas, A. E. Botchkarev, A. Salvador, S. N. Mohammad, and H. Morkoc, J. Appl. Phys. **79**, 7657 (1996).
[21] M. Kamp, M. Mayer, A. Pelzman, A. Thies, H. Chung, H. Sternschulte, O. Marti, and J. Ebeling, Mater. Res. Soc. Symp. Proc. **395**, 135 (1996).
[22] W. Wong, N. Li, H. Dong, F. Deng, S. Lau, C. Tu, J. Hays, S. Bidnyk, and J. Song, J. Cryst. Growth **164**, 159 (1996).
[23] N. Grandjean and J. Massies, Appl. Phys. Lett. **71**, 1816 (1997).
[24] N. Grandjean, J. Massies, M. Leroux, and P. Lorenzini, Appl. Phys. Lett. **72**, 82 (1998).
[25] S. Yoshida, S. Misawa, and A. Itoh, Appl. Phys. Lett. **26**, 461 (1975).
[26] S. Yoshida, S. Misawa, Y. Fujii, S. Takada, S. Gonda, and A. Itoh, J. Vac. Sci. Technol. **16**, 990 (1979).
[27] S. Yoshida, S. Misawa, and S. Gonda, J. Appl. Phys. **53**, 6844 (1982).
[28] S. Yoshida, S. Misawa, and S. Gonda, Appl. Phys. Lett. **42**, 427 (1983).
[29] S. Yoshida, S. Misawa, and S. Gonda, J. Vac. Sci. Technol. B **1**, 250 (1983).
[30] R. C. Powell, N. E. Lee, and J. E. Greene, Appl. Phys. Lett. **60**, 2505 (1992).
[31] J. van der Weide, Ph.D. dissertation, North Carolina State University, 1994.
[32] M. J. Bozack, J. Muehlhoff, J. N. Russel, Jr., W. Choyke, and J. T. Yates, Jr., J. Vac. Sci. Technol. A **5**, 1 (1987).
[33] D. Briggs and M. P. Seah, *Pratical Surface Analysis*, 2nd edition (Wiley, New York, 1990), Vol. 1.
[34] L. M. Porter, R. F. Davis, J. S. Bow, M. J. Kim, R. W. Carpenter, and R. C. Glass, J. Mater. Res. **10**, 668 (1995).
[35] R. Kaplan, Surf. Sci. **215**, 111 (1989).
[36] R. S. Kern and R. F. Davis, Appl. Phys. Lett. **71**, 1356 (1997).
[37] S. W. King, M. Busby, C. Ronning, R. J. Nemanich, and R. F. Davis, J. Appl. Phys. **84**, 6042 (1998).
[38] S. Tanaka, R. S. Kern, and R. F. Davis, Appl. Phys. Lett. **66**, 37 (1995).
[39] M. O. Aboelfotoh, R. S. Kern, S. Tanaka, R. F. Davis, and C. I. Harris, Appl. Phys. Lett. **69**, 2873 (1996).
[40] S. W. King, C. Ronning, R. F. Davis, M. C. Benjamin, and R. J. Nemanich, J. Appl. Phys. **84**, 2086 (1998).
[41] S. W. King, J. P. Barnak, M. D. Bremser, K. M. Tracy, C. Ronning, R. F. Davis, and R. J. Nemanich, J. Appl. Phys. **84**, 5248 (1998).
[42] W. F. Egelhoff, Crit. Rev. Solid State Mater. Sci. **16**, 213 (1990).
[43] S. A. Chambers, Surf. Sci. Rep. **16**, 261 (1992).
[44] T. W. Weeks, Jr., M. D. Bremser, K. S. Ailey, E. Carlson, W. G. Perry, E. L. Piner, N. A. El-Masry, and R. F. Davis, J. Mater. Res. **11**, 1011 (1996).
[45] K. Rapcewicz, M. Nardelli, and J. Bernholc, Phys. Rev. B **56**, 12725 (1997).
[46] S. Krishnankutty, R. M. Kolbas, M. A. Khan, J. N. Kuznia, J. M. Van Hove, and D. T. Olson, J. Electron. Mater. **21**, 437 (1992).
[47] S. Tanaka, R. Kern, J. Bentley, and R. Davis, Jpn. J. Appl. Phys., Part 1 **35**, 1641 (1996).
[48] S. Tanaka, R. Kern, and R. Davis, Appl. Phys. Lett. **66**, 37 (1995).
[49] S. Tanaka, S. Iwai, and Y. Aoyagi, J. Cryst. Growth **170**, 329 (1997).
[50] T. W. Weeks, Jr., M. Bremser, K. Ailey, E. Carlson, W. Perry, and R. Davis, Appl. Phys. Lett. **67**, 410 (1995).
[51] J. Jenny, R. Kaspi, and K. Evans, J. Cryst. Growth **175/176**, 89 (1997).
[52] P. Hacke, G. Feulliet, H. Okumura, and S. Yoshida, Appl. Phys. Lett. **69**, 2507 (1996).
[53] R. Held, D. Crawford, A. Johnston, A. Dabiran, and P. Cohen, J. Electron. Mater. **26**, 272 (1997).
[54] S. Mokler, W. Liu, N. Ohtani, and B. Joyce, Appl. Phys. Lett. **59**, 3419 (1991); Appl. Surf. Sci. **60/61**, 92 (1992); J. Cryst. Growth **120**, 290 (1992).
[55] K. Sakamoto, H. Matsuhata, K. Miki, and T. Sakamoto, J. Cryst. Growth **157**, 295 (1995).
[56] S. Gates and S. Kulkarni, Appl. Phys. Lett. **60**, 53 (1992).
[57] Z. Yu, S. Buczkowski, N. Giles, T. Myers, and M. Richards-Babb, Appl. Phys. Lett. **69**, 2731 (1996).
[58] M. Dresser, P. Taylor, R. Wallace, W. Choyke, and J. Yates, Surf. Sci. **218**, 75 (1989).
[59] S. Tanaka, M. Onchi, and M. Nishijima, Surf. Sci. **191**, L756 (1987).
[60] N. Singh, A. Murrell, D. Harrison, and J. Foord, J. Phys. D **3**, S167 (1991).
[61] D. Parker, M. Jones, and B. Koel, Surf. Sci. **233**, 65 (1990).
[62] M. Schulberg, M. Allendorf, and D. Outka, Surf. Sci. **341**, 262 (1995).
[63] C. Chiang, S. Gates, A. Bensaoula, and J. Schultz, Chem. Phys. Lett. **246**, 275 (1995).
[64] W. Mokwa, D. Kohl, and G. Heiland, Phys. Rev. B **29**, 6709 (1984).
[65] R. Shekhar and K. Jensen, Surf. Sci. **381**, L581 (1997).
[66] H. Liu, D. Bertolet, and J. Rogers, Surf. Sci. **320**, 145 (1994); **340**, 88 (1995).
[67] R. Klauser, P. A. Kumar, and T. Chuang, Surf. Sci. **411**, 329 (1998).
[68] *Concepts and Models of Inorganic Chemistry*, edited by B. Douglas, D. McDaniel, and J. Alexander (Wiley, New York, 1983), p. 78.
[69] G. Schulze and M. Henzler, Surf. Sci. **124**, 336 (1983).
[70] J. Choi, H. Lee, and L. Thompson, Appl. Surf. Sci. **78**, 299 (1994).
[71] A. Winkler, Ch. Resch, and K. Rendulic, J. Chem. Phys. **95**, 7682 (1991); V. Zhukov, A. Ferstl, A. Winkler, and K. Rendulic, Chem. Phys. Lett. **222**, 481 (1994).
[72] E. Kim, I. Berichev, A. Bensaoula, I. Rusakova, K. Waters, and J. Schultz, J. Appl. Phys. **85**, 1178 (1999).